Title: Direct piriform-to-auditory cortical projections shape auditory-olfactory integration

Abbreviated title: Auditory-olfactory integration in auditory cortex

Nathan W. Vogler[1], Ruoyi Chen[1], Alister Virkler[2], Violet Y. Tu[1], Jay A. Gottfried[2], and Maria N. Geffen[1,*]

[1]Department of Otorhinolaryngology, Perelman School of Medicine, University of Pennsylvania

[2]Department of Neurology, Perelman School of Medicine, University of Pennsylvania

*Corresponding Author: mgeffen@pennmedicine.upenn.edu

3450 Hamilton Walk, Stemmler Hall G10, Philadelphia, PA 19104

Number of pages: 46

Number of figures: 6

Number of tables: 1

Number of words: Abstract (169), Introduction (649), Discussion (1283)

Keywords: auditory cortex, piriform cortex, auditory, olfactory, multisensory integration

Conflict of Interest: The authors declare no competing financial interests.

Acknowledgements: Funding: NIH F32MH127788 (to N.W.V.), Kaufman Foundation KA2020-114796 (to M.N.G. and J.A.G.), NIH R01DC015527, NIH R01DC014479, and NIH R01NS113241 (to M.N.G.). The authors would like to thank Tyler Ling for technical assistance.

Abstract

In a real-world environment, the brain must integrate information from multiple sensory modalities, including the auditory and olfactory systems. However, little is known about the neuronal circuits governing how odors influence and modulate sound processing. Here, we investigated the mechanisms underlying auditory-olfactory integration using anatomical, electrophysiological, and optogenetic approaches, focusing on the auditory cortex as a key locus for cross-modal integration. First, retrograde and anterograde viral tracing strategies revealed a direct projection from the piriform cortex to the auditory cortex. Next, using *in vivo* electrophysiological recordings of neuronal activity in the auditory cortex of awake male or female mice, we found that odors modulate auditory cortical responses to sound. Finally, we used *in vivo* optogenetic manipulations during electrophysiology to demonstrate that olfactory modulation in auditory cortex, specifically, odor-driven enhancement of sound responses, depends on direct input from the piriform cortex. Together, our results identify a novel role of piriform-to-auditory cortical circuitry in shaping olfactory modulation in the auditory cortex, shedding new light on the neuronal mechanisms underlying auditory-olfactory integration.

Significance Statement

All living organisms exist within multisensory environments, yet there is a lack in our understanding of how the brain integrates multisensory information. This work highlights a direct piriform-to-auditory cortical circuit governing auditory-olfactory integration. Our results shed new light on a relatively understudied area of multisensory research, promising a more robust understanding of how animals and humans perceive and interact within complex environments.

Introduction

A fundamental role of the central nervous system is to integrate information across multiple sensory modalities to optimize decision-making and behavior. Indeed, rarely does any individual

sensory modality operate alone and unabetted: humans and animals must integrate combinations of sounds, smells, visual input, tactile and proprioceptive information (Gottfried and Dolan, 2003; Deroy et al., 2016; Angeloni and Geffen, 2018; Choi et al., 2018; Wallace et al., 2020). When combining sounds and smells, the brain must integrate information from both the auditory and olfactory systems. Auditory-olfactory integration is an ethologically important domain of multisensory integration. When a cat approaches a mouse, the mouse may use the combination of sounds and smell of the cat to identify it as a predator (Halene et al., 2009). Moreover, combinations of auditory and olfactory stimuli are crucial for pup retrieval behavior in mice, and play critical roles during development — bonds between parents and offspring form based on body odors and vocalization sounds (Marlin and Froemke, 2017; Tasaka et al., 2020; McRae et al., 2023). In humans, the sounds of eating food, such as crunchy potato chips, affect perception of the pleasantness of the food odor, such as potato chip odor/staleness (Seo and Hummel, 2011; Seo et al., 2014). However, the circuits and mechanisms underlying auditory-olfactory integration have remained elusive.

Previous studies examining interactions between audition and olfaction demonstrated cross-modal activation of piriform and auditory cortical areas (Smith et al., 2009; Wesson and Wilson, 2010; Cohen et al., 2011; Varga and Wesson, 2013; Cohen and Mizrahi, 2015; Gnaedinger et al., 2019; Olofsson et al., 2019; Tasaka et al., 2020; Gilday and Mizrahi, 2023; Wu et al., 2023). In the auditory cortex (ACx) of lactating mother mice, pup odors reduce spontaneous activity and increase evoked activity in response to pup ultrasonic vocalizations (Cohen et al., 2011; Cohen and Mizrahi, 2015). Furthermore, learned associations between an odor and a subsequent sound modulate single-neuron responses in the auditory cortex (Gilday and Mizrahi, 2023). Together, these studies suggest that the ACx serves as a locus for auditory-olfactory cross-modal integration, specifically regarding the olfactory modulation of sound processing.

While these studies point to an involvement of the ACx in auditory-olfactory integration, much remains unknown regarding where and how these cross-modal inputs converge. By comparison, previous research on audio-visual integration has found that concurrent visual stimuli improve sound detection and encoding in ACx, facilitated by cross-cortical connections between visual cortex and ACx (Bizley et al., 2016; Atilgan et al., 2018; Meijer et al., 2018; Zhou et al., 2020; Han et al., 2021). Moreover, audio-visual integration crucially depends on the temporal binding of the combined audio-visual stimuli (Meijer et al., 2017, 2019). Similar studies on auditory-olfactory integration have been limited by experimental challenges in delivering combinations of odors and sounds with temporal precision, as well as a lack of knowledge of the brain circuitry underlying auditory-olfactory interactions. Notably, reports of potential cross-modal anatomical connections linking the piriform cortex (Pir) and ACx have been inconsistent. Some have found that neurons in Pir display sound-evoked responses (Varga and Wesson, 2013), and that ACx projects to Pir but not vice versa (Budinger et al., 2006; Budinger and Scheich, 2009). Others have reported a sparse but detectable direct projection from Pir to ACx (Costa et al., 2017; Tasaka et al., 2020), yet its potential role in odor-driven modulation of ACx is unclear. Identifying and characterizing these pathways are important first steps in deciphering how the brain integrates auditory and olfactory stimuli.

Here, we confirm the direct Pir-to-ACx projection using multiple circuit tracing strategies and examine its functional role in auditory-olfactory integration in ACx. We explore the impact of this pathway on olfactory modulation of auditory processing, using a novel experimental setup for delivering odors and sounds with temporal precision to awake mice during *in vivo* electrophysiological recordings in ACx. Our findings reveal that the Pir-to-ACx pathway contributes specifically to odor-mediated enhancement of sound responses in ACx.

Materials and Methods

105 *Mice*

106 For anatomical circuit tracing experiments, we used 5 male C57BL/6J mice (The Jackson
107 Laboratory; strain #000664; RRID:IMSR_JAX:000664; aged 8-16 weeks), 2 male Cdh23 mice
108 (B6N(Cg)-Cdh23$^{tm2.1Kjn}$/Kjn; The Jackson Laboratory, strain #:018399; RRID:IMSR_JAX:018399;
109 aged 22 weeks), and 13 Ai14 Cre reporter mice (progeny of Cdh23 mice crossed with Ai14 mice
110 [B6.Cg-Gt(ROSA)$^{26Sortm14(CAG-tdTomato)Hze}$/J; The Jackson Laboratory, strain #:007914;
111 RRID:IMSR_JAX:007914], 7 male, 6 female, aged 18-26 weeks). For electrophysiological
112 recordings, we used 18 mice: 4 C57BL/6J mice (2 male, 2 female; aged 12-17 weeks at time of
113 recording); and 14 Cdh23 mice (5 male, 9 female; aged 12-26 weeks). Cdh23 mice were used for
114 most experiments because they do not exhibit age-related hearing loss which is common in
115 C57BL/6J mice (Johnson et al., 2017). Any C57BL/6J mice were used by 17 weeks of age. Mice
116 were housed at 28 °C with a 12-h reversed light cycle and food and water provided *ad libitum*.
117 Experiments were performed during the animals' dark cycle. All experimental procedures were
118 approved by the Institutional Care and Use Committee at the University of Pennsylvania and in
119 accordance with National Institutes of Health guidelines.

120

121 *Stereotaxic surgery and virus injections*

122 Mice were anesthetized under isoflurane (1-3%). Prior to surgery, mice were administered
123 subcutaneous doses of buprenorphine (0.05-0.1 mg/kg Buprenex or 1.3 mg/kg Ethiqa),
124 dexamethasone (0.2 mg/kg), and bupivicane (local; 2 mg/kg). A small craniotomy (~1 mm
125 diameter) was made above the respective ACx or Pir injection sites. To label ACx-projecting
126 neurons in Pir in Cdh23 mice, we injected AAVrg-hSyn-eGFP (Addgene #50465-AAVrg;
127 RRID:Addgene_50465; 1.7x10^{13} GC/mL; 250 nL) into left ACx (4.3 mm ML and -2.65 mm AP
128 [relative to Bregma], -0.7 mm DV [relative to brain surface]). To label ACx-projecting neurons in
129 Pir in Ai14 mice, we injected AAVrg-hSyn-Cre-WPRE-hGH (Addgene #105553-AAVrg;
130 RRID:Addgene_105553; 1.9 x10^{13} GC/mL; 150-250 nL) into left ACx. To label Pir-recipient

131 neurons in ACx in Ai14 mice, we injected AAV1-hSyn-Cre-WPRE-hGH (Addgene #105553-AAV1;
132 RRID:Addgene_105553; 1.9 x10^{13} GC/mL; 150-180 nL) into left Pir (3.9 mm ML, -1.5 mm AP, -
133 4.00 DV). Viruses were delivered through 30-40 μm diameter glass micropipettes connected to a
134 syringe pump (Harvard Apparatus Pump 11 Elite; 60 nL/min infusion rate). For optogenetic
135 experiments, in Cdh23 or C57BL/6J mice we injected AAVrg-hSyn-Cre-WPRE-hGH (300 nL) into
136 left ACx and AAV5-hSyn1-SIO-stGtACR1-FusionRed (Addgene #105678-AAV5;
137 RRID:Addgene_105678; 2.1 x10^{13} GC/mL; 300 nL) or AAV5-FLEX-tdTomato (Addgene #28306-
138 AAV5; RRID:Addgene_28306; 2.1 x10^{13} GC/mL; 300 nL) into left Pir (3.9 mm ML, -1.0 mm AP, -
139 4.00 mm DV). A fiber optic cannula (ThorLabs CFML52L05; Ø200 μm Core, 0.50 NA, L=5mm)
140 was implanted over left Pir (3.9 mm ML, -1.0 mm AP, -3.6 mm DV) and secured with dental cement
141 (C&B Metabond). For all electrophysiological recordings, a ground pin was inserted via small
142 craniotomy over the left frontal cortex, and a custom-made stainless steel headplate (eMachine
143 Shop) was secured to the skull using dental cement and acrylic (Lang Dental). After all surgeries,
144 we subcutaneously administered meloxicam (5 mg/kg) and an antibiotic (Baytril 5 mg/kg) for 4
145 days during postoperative care. After virus injections, to allow adequate time for virus expression,
146 we waited at least two weeks (for retrograde tracing/optogenetics) or three weeks (for anterograde
147 tracing) before subsequent recording and/or transcardial perfusion.
148
149 *Histology and cell counting*
150 Mice were anesthetized via intraperitoneal injection of ketamine (120 mg/kg) and
151 dexmedetomidine (1 mg/kg), then perfused with phosphate-buffered saline (PBS) followed by 4%
152 paraformaldehyde (PFA) in PBS. Brains were extracted and immersed in 4% PFA overnight then
153 in 30% sucrose in PBS for at least 36 hours at 4°C. Coronal brain sections (60 μm thickness)
154 were cut on a cryostat (Leica CM1860) at -25°C and mounted on slides using Invitrogen ProLong
155 Antifade Mountant with DAPI. Fluorescent images were acquired using a slide scanning

156 microscope (Zeiss Axio Scan.Z1) under 20x magnification and ZEN 2.3 software. Whole brain
157 fluorescent images were manually aligned with the reference mouse brain atlas (Franklin &
158 Paxinos) to confirm the accuracy of injection sites and extent of viral spread, and to determine
159 regions of interest (ROIs) for cell counting. For the anterior Pir, four coronal sections between 1.0-
160 2.0 mm anterior to Bregma were counted in each mouse. For the posterior Pir, four coronal
161 sections between 1.5-2.5 mm posterior to bregma were counted in each mouse. Fluorescent-
162 labeled cells within ROIs were manually counted using ImageJ software. For ACx subregions,
163 eight coronal sections between 2.2-3.6 mm posterior to bregma were counted in each mouse. A
164 custom-written MATLAB script was used to register the normalized depth of each cell from the
165 pia during manual counting. Specifically, for each ACx subregion, a line segment spanning the
166 depth of the cortex was drawn perpendicular to the pia in the middle of the subregion. The
167 normalized depth for each cell was defined as the relative length of the projection of the cell's
168 location onto that line segment.
169
170 *Electrophysiological recordings*
171 Recordings were performed in a custom-built acoustic isolation booth. At least one week following
172 headplate surgery, mice were habituated to the recording setup for increasing durations (5 – 60
173 min) over the course of 3 days. On the day of recording, mice were anesthetized with 1.5-2.5%
174 isoflurane, and a small craniotomy was made over the left auditory cortex using a dental drill,
175 centered ~1.5mm anterior to the lambdoid suture along the caudal end of the squamosal suture.
176 Following the craniotomy, mice were allowed to recover from anesthesia for at least 30 min. Acute
177 extracellular recordings in ACx were performed using a 32-channel silicon probe (A1x32-Poly2-
178 5mm-50s-177, NeuroNexus). Prior to insertion, the probe was coated in a dye (CM-DiI or SP-DiO;
179 Invitrogen) for post hoc visualization of recording sites. The probe was positioned perpendicularly
180 to the brain surface and lowered at 1-2 μm/s to a final depth of 900-1200 μm or until all channels
181 were within the brain. During lowering of the probe, we monitored responses to brief broadband

noise clicks to confirm localization within auditory cortex. Neuronal signals were amplified and digitized with an Intan headstage (RHD 32ch) and recorded by an OpenEphys acquisition board (Siegle et al., 2017) at a rate of 30 kHz. Signals were filtered between 500 and 6000 Hz, offset corrected, and re-referenced to the median across all channels. Spiking data were sorted using Kilosort2 (Pachitariu et al., 2016) and manually curated in phy2 to identify putative single- and multi-units.

Stimuli

Stimuli during electrophysiological recordings consisted of combinations of auditory and olfactory stimuli. Odors consisted of acetophenone (CAS 98-86-2; Sigma-Aldrich), eucalyptus (100% pure eucalyptus oil; NOW essential oils), or an acetophenone + eucalyptus mixture (1:1 vol/vol), delivered using a respiration-triggered flow dilution olfactometer (Shusterman et al., 2011; Dewan et al., 2018; Williams and Dewan, 2020). We chose these odorants due to their use in previous studies (acetophenone in Cohen et al., 2011), and initially to compare the effects of a monomolecular odorant (acetophenone) versus a more complex mixture (eucalyptus). Because preliminary experiments showed no odor-dependent difference in effects, we combined the groups for subsequent experiments and analysis. This approach allowed us to vary odors between successive recordings in the same mouse, to minimize potential habituation to a single odor. Odorants were liquid diluted 1:1 vol/vol in mineral oil (CAS 8042-47-5; Sigma-Aldrich) in amber vials, then further air diluted (2% N_2/Air) in the olfactometer, for a final dilution of 1%. The control (non-odorant) vial contained pure mineral oil. The olfactometer and stimulus delivery were controlled by custom Python software and Arduino MEGA 2560. Throughout the recording, we monitored the respiratory cycle of the mouse. Respiration (sniffing) was measured non-invasively using a pressure sensor connected via tubing to the odor port around the mouse's nose. The pressure was transduced using the sensor and a preamplifier, and the analog signal from the preamplifier was recorded along with electrophysiological data in OpenEphys. Between each trial,

208 the olfactometer tubing was cleared and primed with the next odor for at least 3 s. At the onset of
209 a trial, the mouse's inhale triggered the 'final valve' to switch from delivering continuous clean
210 background air to odorized air, which rapidly delivered the odorized air to the mouse's nose with
211 no change in total air flow (valve opening duration 1.25 s). Opening of the final valve also triggered
212 playing of the sound stimulus with a delay of 250 ms to allow adequate time for the odor to reach
213 the mouse's nose and subsequent inhale. The onset timing and kinetics of odors were verified
214 using a photo-ionization detector (miniPID; Aurora Scientific). Sounds consisted of 1 s duration
215 broadband gaussian white noise filtered between 3-60 kHz, either unmodulated or amplitude-
216 modulated (10 Hz, 100% modulation depth). Sounds were generated in Python and converted to
217 analog signals via National Instruments card (NI PCIe-6353, 200 kHz sample rate) and delivered
218 through a speaker (MF-1; Tucker-Davis Technologies) pointed toward the mouse's right ear, at 0,
219 45, 55, 65, or 75 dB SPL. Background noise from the olfactometer air flow was measured to be
220 ~50 dB SPL (1/4-inch condenser microphone; Brüel &Kjær). During recordings, on half of trials,
221 we delivered either odorized air or control air. For recordings with optogenetics, on half of trials,
222 we delivered 470 nm LED light (M470F4; ThorLabs) through a fiber optic cannula (ThorLabs
223 CFML52L05; power 2.8-3.7 mW at cannula tip). LED stimulus onset and duration (1.25 s) were
224 the same as final valve opening. For all recordings, trial order was randomized and different for
225 each recording.
226
227 *Electrophysiological data analysis*
228 Neuronal spiking data from each recorded unit were organized by trial type and aligned to the trial
229 onset (i.e. the time of final valve opening). For each unit, peristimulus time histograms (PSTHs)
230 of neuronal spikes were generated using 10 ms time bins, then averaged across trials for each
231 condition. We included all units with baseline firing rate > 1 Hz. For responses to unmodulated
232 noise stimuli, we analyzed spiking during a response window of 0-250 ms after sound onset; for
233 responses to 10 Hz AM stimuli, we analyzed spiking during a response window of 0-1 s. To classify

each unit as sound-responsive or odor-modulated, we input the number of spikes during each trial's response window into a generalized linear model (GLM; predictor variables: sound level [continuous variable normalized from 0-1], odor [0 or 1]; response variable: number of spikes during response window; Poisson distribution, log link function). This allowed the classification of each unit's responses as having a main effect (p<0.05) of sound, odor, and/or a sound-odor interaction. Sound-responsive units that were also responsive to odor or had a significant sound-odor interaction were classified as 'odor-modulated' units. For each odor-modulated unit, to determine the direction and magnitude of olfactory modulation, we calculated an Odor Modulation Index (OMI) according to:

$$OMI = \frac{FR_{Odor} - FR_{Air}}{FR_{Odor} + FR_{Air}}$$

Where FR_{Odor} and FR_{Air} are the mean firing rates in response to sound, with or without odor, respectively. For each unit we calculated the OMI using the mean firing rates for all responses to 5, 15, and 25 dB SNR sounds. Odor-modulated units with OMI>0 were classified as 'enhanced' units; units with OMI<0 were classified as 'suppressed' units. In addition, for both enhanced and suppressed units, we calculated the OMI for each sound level using the responses to each sound stimulus separately. To calculate z-scored firing rates, we used the mean and standard deviation across trials of firing rate during the 1 s baseline period prior to final valve opening. For 'enhanced' units in optogenetics experiments (stGtACR1 and control mice), we calculated an LED Modulation Index according to:

$$LED\ Modulation\ Index = \frac{FR_{Odor\ (LED\ ON)} - FR_{Odor\ (LED\ off)}}{FR_{Odor\ (LED\ ON)} + FR_{Odor\ (LED\ off)}}$$

Where $FR_{Odor\ (LED\ ON)}$ and $FR_{Odor\ (LED\ off)}$ are the mean firing rates in response to Odor+Sound, with or without LED light, respectively.

Sniff data analysis

Raw analog sniff data from each recording were bandpass filtered between 0.5 and 20 Hz, then subsequent analyses were performed on the filtered sniff traces for each trial during the 1.25 s trial duration, as described above. To calculate sniff frequency for each trial, we measured the average time between peaks (exhales) and between troughs (inhales) in the sniff trace. To calculate sniff amplitude for each trial, we measured the difference between the average peak amplitude minus the average trough amplitude.

Statistics

Data analysis and figure generation were performed using Matlab or Python. We used the Shapiro-Wilk test to assess normality. For parametric data we used two-tailed paired or unpaired t-tests between groups; for non-parametric data we used two-tailed Wilcoxon signed-rank or Mann-Whitney tests between groups, or Friedman tests for multiple groups. We performed Bonferroni corrections for multiple comparisons. Significance levels are defined as $p<0.05$. Group data in figures are presented as mean ± SEM, unless otherwise noted. The statistical tests performed are indicated in the text and figure legends. Table 1 contains a detailed summary of statistical tests and comparisons.

Data and code availability

Source data is available on Dryad: https://doi.org/10.5061/dryad.dncjsxm7c. Original code is available on GitHub: https://github.com/geffenlab/Vogler_2024.

Results

The auditory cortex receives direct input from the piriform cortex.

To examine potential anatomical substrates for auditory-olfactory integration in the auditory cortex (ACx), we first sought to identify whether ACx receives direct projections from olfactory brain areas such as the piriform cortex (Pir). We started by injecting a retrograde virus expressing GFP

284 (AAVrg-hSyn-eGFP) into the left ACx of C57BL/6J or Cdh23 mice to selectively label the cell
285 bodies of ACx-projecting neurons (Fig. 1A). We observed fluorescently labeled cells in the
286 ipsilateral Pir (GFP, Fig. 1B). Because the anterior and posterior regions of the Pir are known to
287 exhibit differential long-range connectivity patterns (Bekkers and Suzuki, 2013), we quantified and
288 compared retrograde GFP expression in the anterior Pir (aPir) versus posterior Pir (pPir) (Fig. 1B-
289 C). In most mice, we observed a greater number of labeled cells in pPir compared to aPir. (Fig.
290 1C), suggesting that the Pir-to-ACx projection predominantly arises from pPir. To confirm the
291 accuracy of injection sites, we examined the extent of viral spread in each mouse (Fig. 1D-E),
292 ensuring localization of the virus injection to ACx with minimal spread into surrounding non-
293 auditory regions.
294
295 To further confirm the existence of this projection and validate our approach, we performed a
296 similar retrograde tracing experiment in Ai14 cre-reporter mice (progeny of Cdh23 mice crossed
297 with Ai14 mice), injecting retroAAV expressing Cre (AAVrg-hSyn-Cre) into the ACx (Fig. 1E).
298 Again, we found retrogradely labeled cell bodies in ipsilateral Pir (tdTomato, Fig. 1F), and we
299 observed a significantly greater number of labeled cells in pPir compared to aPir (Fig. 1G,
300 *p=0.020, paired t-test). These retrograde tracing experiments reveal a direct projection to ACx
301 arising from Pir, predominantly from pPir.
302
303 Next, to further characterize Pir input to ACx, we performed anterograde viral tracing to reveal the
304 targets of Pir neurons within ACx. We injected a transsynaptic anterograde virus (Zingg et al.,
305 2020) expressing Cre (AAV1-hSyn-Cre) into the left Pir of Ai14 cre-reporter mice (progeny of
306 Cdh23 mice crossed with Ai14 mice) to selectively label neurons in ACx that receive Pir input (Fig.
307 2A). Because our retrograde tracing experiments (Fig. 1) showed that the Pir-to-ACx projection
308 arises mostly from pPir, we specifically targeted pPir for the anterograde virus injections.
309 Consistent with our retrograde tracing experiments, we observed fluorescently labeled cell bodies

310 in the ipsilateral ACx, including the primary ACx (Au1) and the dorsal and ventral secondary ACx
311 (AuD, AuV) (Fig. 2B-C). We additionally observed Pir-recipient cells in the temporal association
312 cortex (TeA) (Fig. 2B-C), consistent with previous studies (Tasaka et al., 2020). We quantified and
313 compared anterograde tdTomato expression across these cortical subregions and found an
314 increase in the number of labeled cells from dorsal-to-ventral auditory subregions (Fig. 2C,
315 *p=0.014, Friedman test). Furthermore, we quantified the cortical depth of the labeled cells and
316 found that Pir-recipient cells span all layers of ACx, but predominantly in layers 2/3 and 6 (Fig.
317 2D). To again confirm the accuracy of injection sites, we examined the extent of viral spread in
318 each mouse (Fig. 2E), ensuring localization of the virus injection to Pir with minimal spread into
319 surrounding regions. These anterograde tracing experiments further confirm the direct projection
320 from Pir to ACx and reveal that Pir-recipient ACx neurons span auditory cortical and layers and
321 subregions.
322
323 Taken together, our tracing experiments confirm a direct projection from pPir to ACx using multiple
324 retrograde and anterograde viral approaches. Our results are consistent with previous studies
325 showing a sparse but detectable Pir-to-ACx projection (Costa et al., 2017; Tasaka et al., 2020).
326 These results suggest an anatomical substrate by which olfactory sensory information may affect
327 auditory processing in ACx, pointing toward a possible mechanism for auditory-olfactory
328 integration.
329
330 ***In vivo* electrophysiology for assessing auditory-olfactory integration in auditory cortex.**
331 Next, we sought to determine whether and how odors modulate auditory processing in the ACx
332 of awake mice. While previous studies have demonstrated olfactory modulation of sound
333 responses in ACx, most of these studies were performed in anesthetized animals using complex
334 odorants and sound stimuli, or in awake animals but influenced by a behavioral task (Cohen et
335 al., 2011; Cohen and Mizrahi, 2015; Gnaedinger et al., 2019; Gilday and Mizrahi, 2023). As such,

336 it remains unclear how auditory-olfactory integration may depend on brain state, stimulus
337 complexity, and/or experience-dependent learning. We therefore sought to answer the basic
338 question of whether and how a temporally coupled odor modulates ACx responses to simple
339 sounds in untrained, awake mice. To answer this question, we designed a custom-made system
340 combining sound stimuli with a respiration-triggered olfactometer to deliver sounds and odors to
341 awake head-fixed mice with high temporal precision during *in vivo* electrophysiology (Fig. 3A).
342 We recorded the activity of ACx neurons in response to combinations of odor (acetophenone or
343 eucalyptus, 1%) and sound stimuli (unmodulated or amplitude-modulated [AM, 10 Hz] noise, 0 –
344 75 dB). We used the respiration-triggered olfactometer to control the timing of odor/sound stimulus
345 delivery with the mouse's inhale (Fig. 3B). To examine auditory-olfactory integration in ACx, we
346 targeted recordings to the ACx (Fig. 3C) and recorded the activity of single- and multi-units in
347 response to sounds, with or without odor (Fig. 3D).
348
349 Because our anatomical experiments pointed toward the Pir-to-ACx pathway as a possible
350 substrate for auditory-olfactory integration in ACx, we tested whether and how this pathway
351 contributes to odor modulation of sound responses using an *in vivo* optogenetic approach. To
352 selectively inactivate ACx-projecting Pir neurons in C57BL/6J or Cdh23 mice, we injected AAVrg-
353 hSyn-Cre into ACx, and the cre-dependent soma-targeted inhibitory opsin stGtACR1 (AAV5-SIO-
354 stGtACR1) (Mahn et al., 2018) into pPir (Fig. 3E). During *in vivo* recordings, we delivered 470 nm
355 LED light through a fiber optic cannula implanted over pPir (Fig. 3E-F). Fig. 3G-H shows sound
356 responses in an example ACx unit under the various trial conditions: odor enhances the sound
357 responses, but this enhancement is eliminated by LED inactivation of ACx-projecting Pir neurons.
358
359 **Odor modulates sound responses in auditory cortex.**
360 First, we tested whether and how odors modulate responses to sound stimuli in ACx. We identified
361 'sound-responsive' and 'odor-modulated' units using a generalized linear model (GLM). In

362 response to unmodulated broadband noise, ~20% of sound-responsive units were significantly
363 modulated by odor (Fig. 4A). However, the effects of the odor on sound responses were
364 heterogenous: in response to unmodulated noise, we observed both enhancement (Fig. 4B-D,
365 left) and suppression (Fig. 4B-D, right) of sound responses by odor. To quantify the amount of
366 enhancement or suppression in odor-modulated units, we calculated an Odor Modulation Index
367 (OMI) for each unit for each sound level (Fig. 4C). We found that OMIs vary significantly across
368 sound level for enhanced units (Fig. 4C, left; *p=0.039, Friedman test), but not suppressed units
369 (Fig. 4C, right; n.s. p=0.326, Friedman test). Because we used acetophenone and eucalyptus as
370 odorants in our experiments and varied the odor between recordings, we tested for an odor-
371 dependent difference in enhancement or suppression. We compared the amount of odor
372 modulation (OMI) using acetophenone versus eucalyptus (Fig. 4E) and found that odor
373 modulation does not differ between odorants (Fig. 4E, left: n.s. p=0.93, Mann-Whitney test; Fig
374 4E, right: n.s. p=0.63, Mann-Whitney test). Therefore, we combined the groups here and in
375 subsequent experiments and analyses.
376
377 In addition, we tested the effect of odor on responses to 10 Hz amplitude-modulated (AM) noise
378 and performed the same analyses (Fig. 4F-J). In response to AM noise, we found a greater
379 proportion of odor-modulated sound-responsive units (~33%, Fig. 4F). We again observed both
380 enhancement and suppression of sound responses by odor (Fig. 4G-I), and that OMIs vary
381 significantly across sound level for enhanced units (Fig. 4H, left; *p=0.028, Friedman test).
382 Moreover, we again found that odor modulation does not differ between odorants (Fig. 4J, left:
383 n.s. p=0.59, Mann-Whitney test; Fig 4J, right: n.s. p=0.88, Mann-Whitney test).
384
385 In sound-responsive odor-modulated units, we tested the effect of odor on neuronal firing in the
386 absence of sound. We found an overall slight but significant enhancement of neuronal firing rate
387 in response to odor compared to control (Fig. 4K, **p=0.0042, Wilcoxon signed-rank test). This

388 result suggests that odors may impact ACx processing in the absence of sound, as well as in
389 response to sound stimuli. Specifically, odors enhance baseline neuronal firing, but either
390 enhance or suppress sound-evoked responses.
391
392 In response to odors, rodents actively change their respiratory patterns (sniffing) (Wesson et al.,
393 2009; Wachowiak, 2011). To evaluate the potential effects of respiration on the observed changes
394 in neuronal firing in our experiments, we compared the sniff frequency and amplitude during odor
395 versus control trials in each recording (Fig. 4L). We observed that while odor did not significantly
396 affect sniff frequency (Fig. 4L, left; n.s. p=0.28, paired t-test), odor reduced sniff amplitude (Fig.
397 4L, right; ***p=6.7e-7). This may reflect shallower breathing in response to the odor in our
398 experiments. Nevertheless, our results demonstrate odor-evoked changes in ACx activity,
399 enabling further dissection of the underlying mechanisms.
400
401 Together, these results demonstrate that: 1) olfactory stimuli modulate auditory processing in
402 awake mice, including enhancement of baseline firing as well as bidirectional modulation of
403 sound-evoked responses; and 2) olfactory stimuli enhance or suppress neuronal responses to
404 multiple types of sound stimuli, including both unmodulated and AM noise.
405
406 **Piriform input to auditory cortex contributes to auditory-olfactory integration.**
407 To test the role of the newly characterized Pir-to-ACx pathway (Fig. 1-2) in auditory-olfactory
408 olfactory integration, we combined *in vivo* electrophysiology in awake mice with optogenetics
409 specifically targeting ACx-projecting Pir neurons (Fig. 3). We again recorded sound responses
410 with or without odor, but now we also optogenetically inactivated ACx-projecting Pir neurons by
411 shining LED light through a cannula implanted over ipsilateral pPir (Fig. 3E-H). Consistent with
412 our previous experiments (Fig. 4), we observed both enhancement and suppression of sound
413 responses by odor in a subpopulation of ACx units (Fig. 5A). For both the enhanced and

414 suppressed units, we compared the amount of odor modulation, using the OMI, with or without
415 LED-inactivation of Pir neurons. Strikingly, we observed that for the enhanced units, the LED
416 significantly reduced odor modulation (**p=0.001, Wilcoxon signed-rank test), whereas odor
417 modulation in suppressed units was unaffected (n.s. p=0.96, Wilcoxon signed-rank test) (Fig. 5A).
418 We then examined the effect of the LED on odor modulation for each sound level (Fig. 5B-C) and
419 found that in enhanced units, the LED significantly reduced the amount of odor modulation (OMI)
420 at the highest sound level (Fig. 5C, left; 25 dB SNR: *p=0.042, Wilcoxon signed-rank test),
421 whereas in suppressed units the odor modulation was unaffected (Fig. 5C, right; 25 dB SNR: n.s.
422 p=0.73, Wilcoxon signed-rank test). We again repeated the same analyses for responses to AM
423 noise and observed similar results: the LED significantly reduced the amount of odor modulation
424 in enhanced units (**p=0.004, Wilcoxon signed-rank test), but not in suppressed units (n.s.
425 p=0.63, Wilcoxon signed-rank test) (Fig. 5E). For enhanced units, the LED significantly reduced
426 the amount of odor modulation at 15 dB SNR and 25 dB SNR (Fig. 5G, left; 15 dB SNR: *p=0.013;
427 25 dB SNR: *p=0.021; Wilcoxon signed-rank tests), whereas suppressed units were unaffected
428 (Fig. 5G, right; 15 dB SNR: n.s. p=0.10, Wilcoxon signed-rank test; 25 dB SNR: n.s. p=0.23,
429 paired t-test). These results demonstrate that odor *enhancement* of sound responses, but not
430 odor suppression, requires the Pir-to-ACx pathway, suggesting that this pathway provides an
431 excitatory drive.
432
433 In addition, we examined odor-driven enhancement of ACx neuronal firing in the absence of
434 sound, with or without *in vivo* optogenetic inactivation of Pir neurons. Consistent with our previous
435 experiments (Fig. 4K), in odor-modulated ACx units we observed that odor significantly enhanced
436 neuronal firing rate, compared to control (Fig. 5I, left; LED off: ***p=3.07e-7, paired t-test).
437 Strikingly, however, this enhancement was eliminated by the LED (Fig. 5I, left; LED ON, n.s. p>1,
438 Wilcoxon signed-rank test). When comparing the amount of odor modulation (OMI) with versus
439 without the LED, we found that the LED significantly reduced the odor-driven enhancement in the

440 absence of sound (Fig. 5I, middle; ***p=2.3e-7, Wilcoxon signed-rank test). This result suggests
441 that optogenetic inactivation of ACx-projecting Pir neurons eliminates odor-driven enhancement
442 of baseline ACx neuronal firing, and therefore that this enhancement requires the direct Pir-to-
443 ACx pathway.
444
445 Finally, we examined potential effects of respiration on the changes in neuronal firing we observed
446 in our optogenetic experiments (Fig. 5J). Consistent with our previous results (Fig. 4L), we
447 observed an odor-mediated reduction of sniff amplitude (Fig. 5J, right; LED off, ***p=6.2e-5,
448 Wilcoxon signed-rank test) but not sniff frequency (Fig. 5J, left; LED off, n.s. p=0.087, paired t-
449 test). Importantly, during trials with the LED, we observed similar effects (Fig. 5J, right: LED ON,
450 ***p=0.0004, Wilcoxon signed-rank test; Fig. 5J, left: LED ON, n.s. p=0.076, paired t-test).
451 Moreover, when comparing respiration during odor trials with versus without the LED, we
452 observed that the LED did not affect sniff frequency (Fig. 5J, left; n.s. p=0.78, paired t-test) or
453 amplitude (Fig. 5J, right, n.s. p=0.35, Wilcoxon signed-rank test). These results critically
454 demonstrate that the optogenetic reduction of odor-driven enhancement is not due to any effects
455 of the LED on sniffing, and is likely specifically due to inactivation of the Pir-to-ACx pathway.
456
457 To further confirm that the optogenetic effects we observed (Fig. 5) were specifically due to
458 inactivation of Pir-to-ACx input via light activation of stGtACR1, and not potential other non-
459 specific effects of the LED light, we performed additional control experiments. Control Cdh23 mice
460 underwent an identical experimental procedure as the optogenetic mice, except we injected a
461 control virus into Pir (AAV5-Flex-tdTomato) instead of opsin (Fig. 6A). In control mice, LED light
462 did not significantly reduce odor modulation in enhanced units, for both unmodulated noise (Fig.
463 6B-C, left; n.s. p=0.11, Wilcoxon signed-rank test) and AM noise (Fig. 6B-C, right; n.s. 0.115,
464 Wilcoxon signed-rank test). Next, we examined the effect of the LED on enhanced units in the
465 controls. To quantify the effect of the LED on olfactory modulation, we calculated an LED

466 Modulation Index (Fig. 6E). For both unmodulated noise (Fig. 6E, left; **p=0.01, Mann-Whitney
467 test) and AM noise (Fig. 6E, right; *p=0.037, Mann-Whitney test), the LED significantly reduced
468 odor modulation in mice expressing stGtACR1 as compared to controls.
469
470 In control mice we again observed odor-driven enhancement of baseline neuronal firing in the
471 absence of sound (Fig. 6F, left; LED off, ***p=8.7e-9, paired t-test); however, this enhancement
472 persisted with the LED (Fig. 6F, left; LED ON, ***p=1.64e-6, Wilcoxon signed-rank test). When
473 comparing the amount of odor modulation (OMI) with versus without the LED, we found that the
474 LED did not affect the odor-driven enhancement in the absence of sound (Fig. 6F, right; n.s.
475 p=0.31, Wilcoxon signed-rank test). Additionally, when comparing respiration during the various
476 stimulation conditions, we again confirmed that the LED did not affect sniff frequency (Fig. 6G,
477 left; n.s. p>1, Wilcoxon signed-rank test) or amplitude (Fig. 6G, right; n.s. p=0.40, Wilcoxon
478 signed-rank test). These results confirm that the reduction of odor-driven enhancement we
479 observed in mice expressing stGtACR1 (Fig. 5) was specifically due to inactivation of the Pir-to-
480 ACx pathway.
481
482 Together, our results identify the role of the Pir-to-ACx pathway in auditory-olfactory integration.
483 Optogenetic inactivation of ACx-projecting Pir neurons selectively reduced odor-driven
484 enhancement of baseline ACx firing as well as enhancement of sound-evoked responses.
485 Therefore, the Pir-to-ACx pathway contributes to odor-mediated enhancement of sound
486 responses, but not suppression.
487
488 **Discussion**
489 In this study we tested the functional role of a direct projection from the piriform cortex to the
490 auditory cortex. We identified the Pir-to-ACx pathway using retrograde and anterograde viral
491 tracing, highlighting that this pathway arises primarily from posterior Pir (Fig. 1), and projects to

492 multiple ACx subregions and laminae (Fig. 2). Next, using *in vivo* electrophysiology in ACx, we
493 demonstrated that olfactory stimuli enhance baseline activity in ACx neurons and bidirectionally
494 modulate sound-evoked activity, either enhancing or suppressing sound responses (Figs. 3-4).
495 Finally, using *in vivo* optogenetics during electrophysiology, we found that the Pir-to-ACx
496 projection is necessary for odor-mediated enhancement of ACx activity and sound responses, but
497 is minimally engaged during suppression (Figs. 5-6). Our results reveal that the Pir-to-ACx
498 pathway shapes auditory-olfactory integration in ACx, contributing to odor-mediated
499 enhancement of sound processing.
500
501 Our anatomical results demonstrate that the Pir-to-ACx projection primarily arises from posterior
502 Pir (pPir), and projects across multiple ACx subregions and cortical layers. Its origination in pPir
503 is consistent with previous studies showing that pPir contains more associational connections
504 with other higher-order brain areas compared to anterior Pir (Bekkers and Suzuki, 2013). For
505 example, pPir is known to have interconnections with the prefrontal cortex, amygdala, and
506 entorhinal and perirhinal cortices, and is thought to encode odor quality (Johnson et al., 2000;
507 Zelano et al., 2011). Our results add ACx to the list of Pir-recipient regions and expand knowledge
508 of cross-modal cortical circuitry. Moreover, the distribution of Pir-recipient neurons spanning ACx
509 is consistent with previous studies showing that cortico-cortical intra-telencephalic neurons
510 project to/from multiple cortical layers including L2/3 and L6 (Shepherd, 2013; Harris and
511 Shepherd, 2015).
512
513 Notably, while previous studies have shown evidence for the Pir-to-ACx projection (Costa et al.,
514 2017; Tasaka et al., 2020), such findings have gone relatively underexplored. Our results are
515 consistent with these previous studies and provide further evidence for the existence and
516 functional impact of the Pir-to-ACx cross-cortical circuit. Although this projection is sparse, we
517 revealed this circuity using a rigorous approach comprised of four different viral strategies:

518 retroAAV-GFP (Fig. 1), retroAAV-Cre (Fig. 1), AAV1-Cre (Fig. 2), and selective labeling of ACx-
519 projecting Pir neurons for optogenetics (retroAAV-Cre and AAV5-stGtACR1, Fig. 3). It is possible
520 that a few Pir cells labeled as ACx-projecting (Fig. 1) or Pir-recipient ACx cells (Fig. 2) may instead
521 result from minor viral spread outside the target region (Fig. 1D-E, 2E); however, our redundant
522 approach increases our confidence in our results revealing the Pir-to-ACx pathway, which are
523 also consistent with some previous studies (Costa et al., 2017; Tasaka et al., 2020). Yet while our
524 experiments yielded robust and reproducible results using these strategies, the question remains
525 why some other research groups previously did not observe this projection. One explanation could
526 simply relate to differences in the tracer used (retroAAVs here versus fluorescein-labeled dextran
527 (Budinger et al., 2006; Budinger and Scheich, 2009)) and/or the animal model (mice here versus
528 gerbils (Budinger et al., 2006; Budinger and Scheich, 2009)). In addition, due to the sparseness
529 of the Pir-to-ACx projection, it is possible that this pathway may have gone unnoticed in some
530 previous studies in which it was not the target of investigation.
531
532 Some previous rodent studies examined auditory-olfactory integration in ACx, providing an
533 important foundation for understanding where and how the brain integrates auditory and olfactory
534 stimuli (Cohen et al., 2011; Cohen and Mizrahi, 2015; Gilday and Mizrahi, 2023). Our data build
535 upon this foundation and underscore modulation of sound responses by odors in naïve, passively
536 exposed, awake mice. Previous experiments using more complex stimuli, such as modulation of
537 ACx responses to pup vocalizations by pup odors, used acetophenone as a control odor stimulus,
538 showing no effect on sound responses (Cohen et al., 2011). That said, the Cohen et al. study was
539 performed in anesthetized animals, and it has since been well-established that neuronal
540 responses vary greatly in anesthetized versus awake states (Fontanini and Katz, 2008; Lesicko
541 et al., 2022). Our results suggest that olfactory modulation by simple odorants such as
542 acetophenone may depend on brain state. Furthermore, the combined olfactory and auditory
543 stimuli in previous studies were not bound precisely in time, and often involved other factors such

544 as behavioral training and associative learning that could have altered cross-modal coding
545 (Cohen et al., 2011; Cohen and Mizrahi, 2015; Gilday and Mizrahi, 2023). Our results in passively
546 exposed, untrained mice suggest that auditory-olfactory integration in ACx does not require
547 behavioral training. Future studies will be needed to further disentangle the complex relationships
548 between brain state, stimulus complexity, and experience-dependent learning involved in
549 auditory-olfactory integration and its neurophysiological underpinnings. Interestingly, an important
550 recent study has suggested that auditory-olfactory integration occurs in higher-order areas of
551 entorhinal cortex due to shared auditory and olfactory inputs (Wu et al., 2023). Our results add to
552 this growing body of literature and suggest that auditory-olfactory integration occurs at even
553 earlier stages in the sensory processing hierarchy than previously realized.
554
555 In sound-responsive odor-modulated units, we found that odor alone produces a slight
556 enhancement of firing rate even in the absence of sound (Figs. 4K, 5I, 6F). Thus, olfactory input
557 may affect both baseline and sound-evoked ACx activity. Our findings of both enhanced and
558 suppressed sound-evoked responses are consistent with previous studies in other modalities
559 such as in audio-visual integration, showing that visual stimuli evoke both excitation and
560 modulation of ACx (Bizley et al., 2007; Kayser et al., 2008; Atilgan et al., 2018). However, the
561 relatively modest degree of the odor-mediated effects on ACx activity observed here (Figs. 3-6),
562 coupled with the sparse nature of the Pir-to-ACx projection (Figs. 1-2), overall suggest that this
563 olfactory input to ACx likely sculpts auditory processing in ACx, rather than providing a strong
564 excitatory drive.
565
566 We found that Pir input to ACx contributes to odor-mediated enhancement of baseline and sound-
567 evoked responses, but not suppression of sound-evoked responses. It is intriguing to consider
568 what mechanism might account for this dichotomy. Because most long-range intra-telencephalic
569 projections are excitatory (Shepherd, 2013; Harris and Shepherd, 2015), odor enhancement may

be due to activation of ACx by direct Pir input, whereas odor suppression may arise from indirect input via local circuitry or via other brain regions. In our anterograde tracing experiments identifying Pir-recipient neurons, we observed that the TeA receives a large amount of Pir input (Fig. 2), a finding that is consistent with previous studies (Tasaka et al., 2020, 2023) and suggests that TeA is a region that might relay Pir input to ACx, ultimately affecting ACx activity. Together these results pave the way for future studies to disentangle the relative contributions of direct Pir input versus indirect pathways to auditory-olfactory integration in ACx, and how the Pir-to-ACx pathway interacts with other multimodal and higher-order brain circuity.

Finally, it is worth noting that previous studies of auditory-olfactory integration have largely focused on parental behavior, including the effects of pup odors on auditory processing in maternal mice, as well as pup retrieval (Cohen and Mizrahi, 2015; Marlin et al., 2015; Marlin and Froemke, 2017; McRae et al., 2023). Moving forward, it will be interesting to determine the extent to which the Pir-to-ACx pathway may contribute to parental behavior, pup retrieval, and other complex behaviors. Although our present study has focused on the effects of simple neutral odorants, future studies are poised to investigate the additional effects of ethologically relevant odors, such as pup odors, social odors, food odors, or predator odors. Furthermore, auditory-olfactory integration in ACx is known to undergo plasticity during motherhood as well as during formation of odor-sound associations (Cohen and Mizrahi, 2015; Gnaedinger et al., 2019; Gilday and Mizrahi, 2023). Drawing from these findings, we suggest that the Pir-to-ACx pathway serves as a novel contributor to multimodal processing that may play a role in multisensory plasticity and learning.

References

Angeloni C, Geffen MN (2018) Contextual modulation of sound processing in the auditory cortex. Curr Opin Neurobiol 49:8–15 Available at:

www.sciencedirect.comwww.sciencedirect.com [Accessed November 18, 2020].

Atilgan H, Town SM, Wood KC, Jones GP, Maddox RK, Lee AKC, Bizley JK (2018) Integration of Visual Information in Auditory Cortex Promotes Auditory Scene Analysis through Multisensory Binding. Neuron 97:640-655.e4 Available at: https://doi.org/10.1016/j.neuron.2017.12.034 [Accessed December 7, 2020].

Bekkers JM, Suzuki N (2013) Neurons and circuits for odor processing in the piriform cortex. Trends Neurosci 36:429–438.

Bizley JK, Jones GP, Town SM (2016) Where are multisensory signals combined for perceptual decision-making? Curr Opin Neurobiol 40:31–37 Available at: http://dx.doi.org/10.1016/j.conb.2016.06.003 [Accessed November 18, 2020].

Bizley JK, Nodal FR, Bajo VM, Nelken I, King AJ (2007) Physiological and anatomical evidence for multisensory interactions in auditory cortex. Cereb Cortex 17:2172–2189.

Budinger E, Heil P, Hess A, Scheich H (2006) Multisensory processing via early cortical stages: Connections of the primary auditory cortical field with other sensory systems. Neuroscience 143:1065–1083.

Budinger E, Scheich H (2009) Anatomical connections suitable for the direct processing of neuronal information of different modalities via the rodent primary auditory cortex. Hear Res 258:16–27.

Choi I, Lee JY, Lee SH (2018) Bottom-up and top-down modulation of multisensory integration. Curr Opin Neurobiol 52:115–122 Available at: https://doi.org/10.1016/j.conb.2018.05.002.

Cohen L, Mizrahi A (2015) Plasticity during motherhood: Changes in excitatory and inhibitory layer 2/3 neurons in auditory cortex. J Neurosci 35:1806–1815.

Cohen L, Rothschild G, Mizrahi A (2011) Multisensory integration of natural odors and sounds in the auditory cortex. Neuron 72:357–369.

Costa NM da, Martin KAC, Sägesser FD (2017) A weighted graph of the projections to mouse auditory cortex. bioRxiv:228726.

622 Deroy O, Faivre N, Lunghi C, Spence C, Aller M, Noppeney U (2016) The Complex Interplay
623 between Multisensory Integration and Perceptual Awareness. Multisens Res 29:585–606.
624 Dewan A, Cichy A, Zhang J, Miguel K, Feinstein P, Rinberg D, Bozza T (2018) Single olfactory
625 receptors set odor detection thresholds. Nat Commun 9:1–12 Available at:
626 http://dx.doi.org/10.1038/s41467-018-05129-0.
627 Fontanini A, Katz DB (2008) Behavioral states, network states, and sensory response variability.
628 J Neurophysiol 100:1160–1168.
629 Gilday OD, Mizrahi A (2023) Learning-Induced Odor Modulation of Neuronal Activity in Auditory
630 Cortex. J Neurosci 43:1375–1386.
631 Gnaedinger A, Gurden H, Gourévitch B, Martin C (2019) Multisensory learning between odor
632 and sound enhances beta oscillations. Sci Rep 9:11236.
633 Gottfried JA, Dolan RJ (2003) The nose smells what the eye sees: Crossmodal visual facilitation
634 of human olfactory perception. Neuron 39:375–386.
635 Halene TB, Talmud J, Jonak GJ, Schneider F, Siegel SJ (2009) Predator odor modulates
636 auditory event-related potentials in mice. Neuroreport 20:1260–1264.
637 Han X, Xu J, Chang S, Keniston L, Yu L (2021) Multisensory-Guided Associative Learning
638 Enhances Multisensory Representation in Primary Auditory Cortex. Cereb Cortex:1–15.
639 Harris KD, Shepherd GMG (2015) The neocortical circuit: Themes and variations. Nat Neurosci
640 18:170–181.
641 Johnson DMG, Illig KR, Behan M, Haberly LB (2000) New features of connectivity in piriform
642 cortex visualized by intracellular injection of pyramidal cells suggest that “primary” olfactory
643 cortex functions like “association” cortex in other sensory systems. J Neurosci 20:6974–
644 6982.
645 Johnson KR, Tian C, Gagnon LH, Jiang H, Ding D, Salvi R (2017) Effects of Cdh23 single
646 nucleotide substitutions on age-related hearing loss in C57BL/6 and 129S1/Sv mice and
647 comparisons with congenic strains. Sci Rep 7:1–13.

648 Kayser C, Petkov CI, Logothetis NK (2008) Visual modulation of neurons in auditory cortex.
649 Cereb Cortex 18:1560–1574.
650 Lesicko AMH, Angeloni CF, Blackwell JM, De Biasi M, Geffen MN (2022) Cortico-Fugal
651 Regulation of Predictive Coding. Elife 11:1–29.
652 Mahn M, Gibor L, Patil P, Cohen-Kashi Malina K, Oring S, Printz Y, Levy R, Lampl I, Yizhar O
653 (2018) High-efficiency optogenetic silencing with soma-targeted anion-conducting
654 channelrhodopsins. Nat Commun 9 Available at: http://dx.doi.org/10.1038/s41467-018-
655 06511-8.
656 Marlin BJ, Froemke RC (2017) Oxytocin modulation of neural circuits for social behavior. Dev
657 Neurobiol 77:169–189.
658 Marlin BJ, Mitre M, D'Amour JA, Chao M V, Froemke RC (2015) Oxytocin enables maternal
659 behaviour by balancing cortical inhibition. Nature 520:499–504.
660 McRae BR, Andreu V, Marlin BJ (2023) Integration of olfactory and auditory cues eliciting
661 parental behavior. J Neuroendocrinol:1–11.
662 Meijer GT, Mertens PEC, Pennartz CMA, Olcese U, Lansink CS (2019) The circuit architecture
663 of cortical multisensory processing: Distinct functions jointly operating within a common
664 anatomical network. Prog Neurobiol 174:1–15 Available at:
665 https://doi.org/10.1016/j.pneurobio.2019.01.004.
666 Meijer GT, Montijn JS, Pennartz CMA, Lansink CS (2017) Audiovisual modulation in mouse
667 primary visual cortex depends on cross-modal stimulus configuration and congruency. J
668 Neurosci 37:8783–8796.
669 Meijer GT, Pie JL, Dolman TL, Pennartz CMA, Lansink CS (2018) Audiovisual integration
670 enhances stimulus detection performance in mice. Front Behav Neurosci 12:231 Available
671 at: https://www.frontiersin.org/article/10.3389/fnbeh.2018.00231/full [Accessed November
672 18, 2020].
673 Olofsson JK, Zhou G, East BS, Zelano C, Wilson DA (2019) Odor identification in rats:

Behavioral and electrophysiological evidence of learned olfactory-auditory associations. eNeuro 6 Available at: https://doi.org/10.1523/ENEURO.0102-19.2019 [Accessed July 1, 2020].

Pachitariu M, Steinmetz N, Kadir S, Carandini M, Harris KD (2016) Kilosort: realtime spike-sorting for extracellular electrophysiology with hundreds of channels. bioRxiv:061481 Available at: http://biorxiv.org/lookup/doi/10.1101/061481.

Seo H-S, Hummel T (2011) Auditory-Olfactory Integration: Congruent or Pleasant Sounds Amplify Odor Pleasantness. Chem Senses 36:301–309 Available at: https://academic.oup.com/chemse/article/36/3/301/506704 [Accessed November 24, 2020].

Seo H-S, Lohse F, Luckett CR, Hummel T (2014) Congruent Sound Can Modulate Odor Pleasantness. Chem Senses 39:215–228 Available at: https://academic.oup.com/chemse/article/39/3/215/502704 [Accessed November 24, 2020].

Shepherd GMG (2013) Corticostriatal connectivity and its role in disease. Nat Rev Neurosci 14:278–291 Available at: www.nature.com/reviews/neuro [Accessed October 15, 2020].

Shusterman R, Smear MC, Koulakov AA, Rinberg D (2011) Precise olfactory responses tile the sniff cycle. Nat Neurosci 14:1039–1044.

Siegle JH, López AC, Patel YA, Abramov K, Ohayon S, Voigts J (2017) Open Ephys: An open-source, plugin-based platform for multichannel electrophysiology. J Neural Eng 14.

Smith JJ, Shionoya K, Sullivan RM, Wilson DA (2009) Auditory stimulation dishabituates olfactory responses via noradrenergic cortical modulation. Neural Plast 2009.

Tasaka G ichi, Feigin L, Maor I, Groysman M, DeNardo LA, Schiavo JK, Froemke RC, Luo L, Mizrahi A (2020) The Temporal Association Cortex Plays a Key Role in Auditory-Driven Maternal Plasticity. Neuron 107:566-579.e7 Available at: https://doi.org/10.1016/j.neuron.2020.05.004.

700 Tasaka G ichi, Maggi C, Taha E, Mizrahi A (2023) The local and long-range input landscape of
701 inhibitory neurons in mouse auditory cortex. J Comp Neurol 531:502–514.
702 Varga AG, Wesson DW (2013) Distributed auditory sensory input within the mouse olfactory
703 cortex. Eur J Neurosci 37:564–571.
704 Wachowiak M (2011) All in a Sniff: Olfaction as a Model for Active Sensing. Neuron 71:962–973
705 Available at: http://dx.doi.org/10.1016/j.neuron.2011.08.030.
706 Wallace MT, Woynaroski TG, Stevenson RA (2020) Multisensory integration as a window into
707 orderly and disrupted cognition and communication. Annu Rev Psychol 71:193–219
708 Available at: https://doi.org/10.1146/annurev-psych-010419- [Accessed November 20,
709 2020].
710 Wesson DW, Verhagen J V., Wachowiak M (2009) Why sniff fast? The relationship between
711 sniff frequency, odor discrimination, and receptor neuron activation in the rat. J
712 Neurophysiol 101:1089–1102.
713 Wesson DW, Wilson DA (2010) Smelling sounds: Olfactory-auditory sensory convergence in the
714 olfactory tubercle. J Neurosci 30:3013–3021.
715 Williams E, Dewan A (2020) Olfactory detection thresholds for primary aliphatic alcohols in
716 mice. Chem Senses 45:513–521.
717 Wu T, Li S, Du D, Li R, Liu P, Yin Z, Zhang H, Qiao Y, Li A (2023) Olfactory–auditory sensory
718 integration in the lateral entorhinal cortex. Prog Neurobiol 221:102399 Available at:
719 https://doi.org/10.1016/j.pneurobio.2022.102399.
720 Zelano C, Mohanty A, Gottfried JA (2011) Olfactory Predictive Codes and Stimulus Templates
721 in Piriform Cortex. Neuron 72:178–187 Available at:
722 http://dx.doi.org/10.1016/j.neuron.2011.08.010.
723 Zhou H yu, Cheung EFC, Chan RCK (2020) Audiovisual temporal integration: Cognitive
724 processing, neural mechanisms, developmental trajectory and potential interventions.
725 Neuropsychologia 140 Available at:

726 https://doi.org/10.1016/j.neuropsychologia.2020.107396 [Accessed November 20, 2020].
727 Zingg B, Peng B, Huang J, Tao HW, Zhang LI (2020) Synaptic specificity and application of
728 anterograde transsynaptic AAV for probing neural circuitry. J Neurosci 40:3250–3267
729 Available at: https://doi.org/10.1523/JNEUROSCI.2158-19.2020 [Accessed October 15,
730 2020].
731

732 **Figures and Legends**

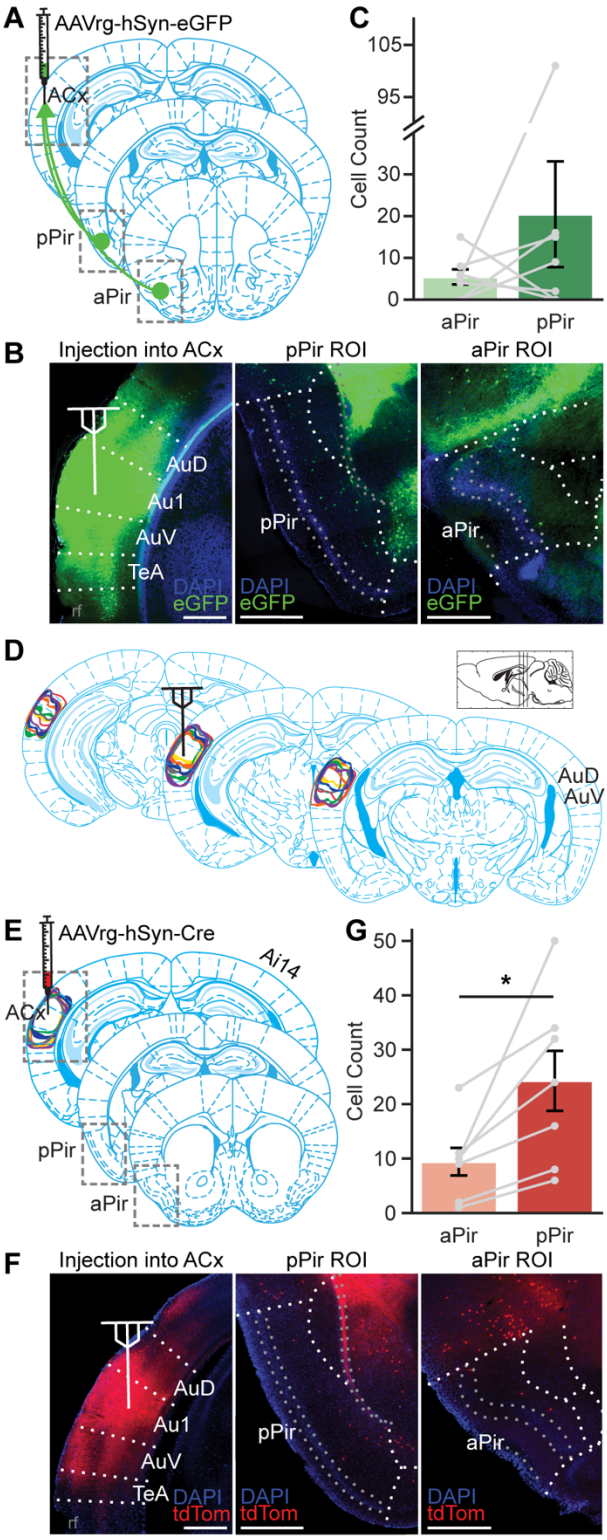

733

734 **Figure 1. Neurons in the ipsilateral piriform cortex directly project to the auditory cortex.**
735 **A)** Injection of AAVrg-hSyn-eGFP into the left auditory cortex (ACx) of C57BL/6J mice (n=5) or
736 Cdh23 mice (n=2). **B)** Representative fluorescent micrographs of ACx injection site (left), posterior
737 piriform (pPir) ROI (middle), anterior piriform (aPir) ROI (right). Scale bars = 500 μm. **C)** Number
738 of cells labeled with GFP in aPir and pPir (n=7 mice; n.s. Wilcoxon signed-rank test). **D)** Viral
739 spread around ACx injection site. Colored outlines indicate extent of viral spread for each mouse
740 (n=7 mice). From left to right, atlas overlays are bregma -3.08 mm, -2.54 mm, and -2.06 mm. **E)**
741 Injection of AAVrg-hSyn-Cre into the left ACx of Ai14 mice (n=7). Colored outlines indicate extent
742 of viral spread around each ACx injection site (n=7 mice). **F)** Representative fluorescent
743 micrographs of ACx injection site (left), pPir ROI (middle), aPir ROI (right). Scale bars = 500 μm.
744 **G)** Number of cells labeled with tdTomato in aPir and pPir (n=7 mice; *$p<0.05$, paired t-test).

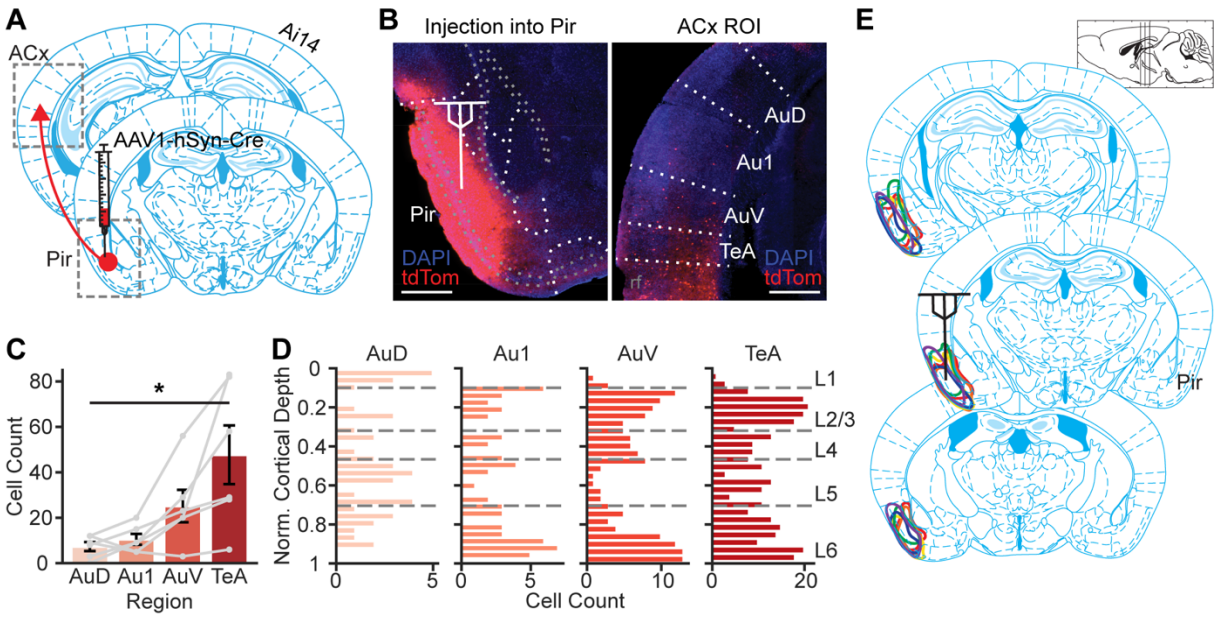

Figure 2. Neurons that receive piriform cortical input span auditory cortical regions. A) Injection of AAV1-hSyn-Cre into the left piriform cortex (Pir) of Ai14 mice (n=6). **B)** Representative fluorescent micrographs of the Pir injection site (left) and auditory cortical ROIs (right). Scale bars = 500 μm. **C)** Number of cells labeled with tdTomato across auditory cortical regions (n=6 mice; *p<0.05, Friedman test). **D)** Histograms of the depth distribution (normalized cortical depth) of labeled cells in each auditory cortical region (all cells from 6 mice). **E)** Viral spread around Pir injection site. Colored outlines indicate extent of viral spread for each mouse (n=6 mice). From top to bottom, atlas overlays are bregma -1.94 mm, -1.46 mm, and -0.94 mm.

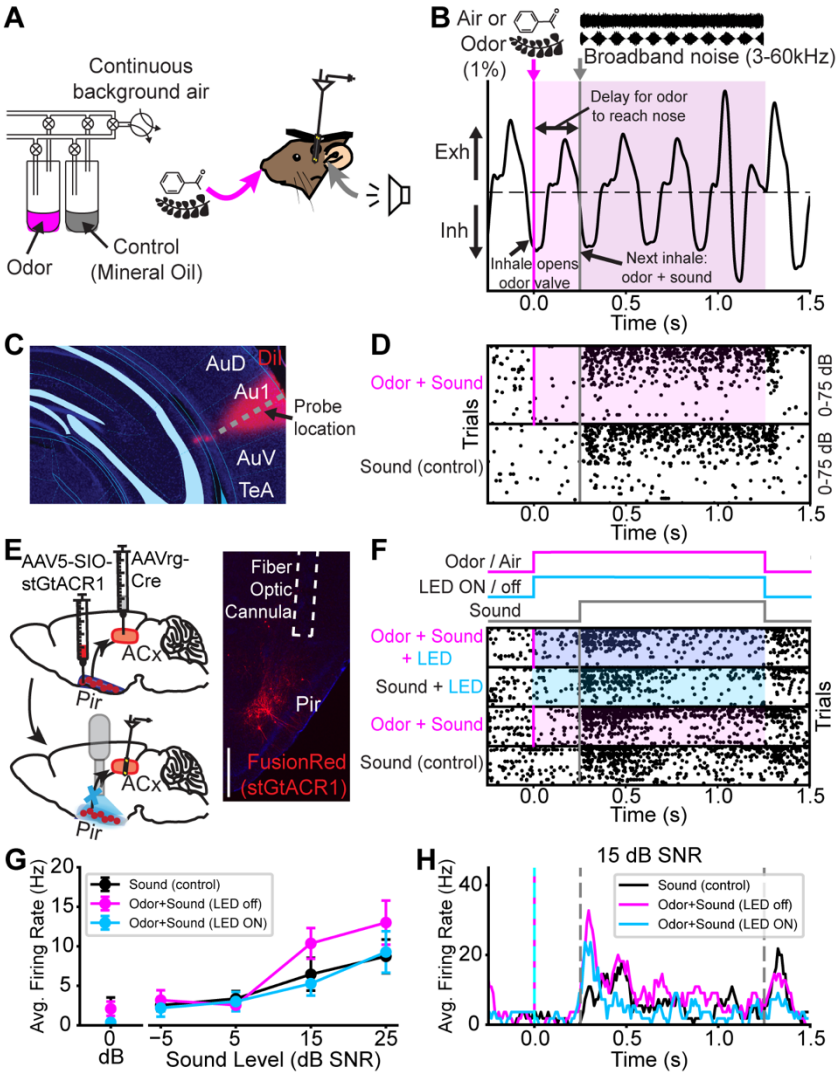

754

755 **Figure 3. *In vivo* electrophysiology for assessing auditory-olfactory integration in auditory**
756 **cortex. A)** Experimental setup for delivering combinations of odor/sounds to awake mice during
757 recordings. **B)** Stimulus timing using respiration-triggered olfactometer. **C)** Example post-hoc
758 visualization of probe location using DiI. **D)** Example raster plot from sound-responsive ACx unit.
759 Trials sorted by sound intensity and odor/control**. E)** Virus injections for selectively expressing
760 stGtACR1 in ACx-projecting Pir neurons in C57BL/6J or Cdh23 mice. Right: example opsin
761 expression in Pir and cannula placement for in vivo optogenetics using 470 nm LED. Scale bar =
762 500 µm. **F)** Stimulus timing during optogenetic experiments and example raster plot from ACx
763 unit. Trials sorted by sound intensity and odor/LED combination. **G)** Average firing rates (Hz) of

764 example unit shown in F, in response to various sound levels (left: 0 dB [no sound]; right: dB SNR
765 [relative to background noise of olfactometer air flow]) in control and odor, with and without LED
766 inactivation of PCx-to-ACx projections. **H)** Peristimulus time histogram (PSTH) of example unit
767 shown in F and G, in response to 15 dB SNR sound.

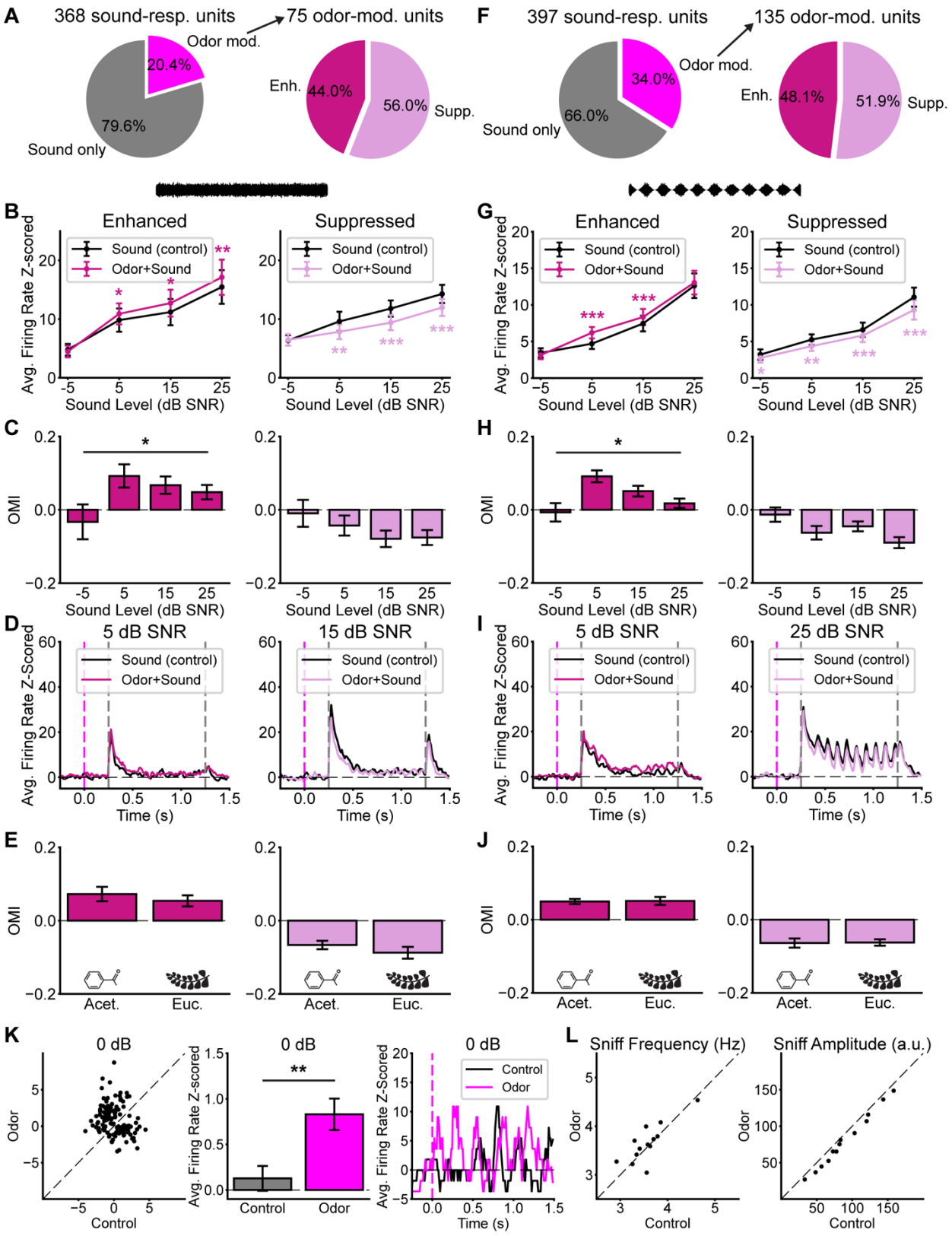
A
368 sound-resp. units
75 odor-mod. units
Odor mod.
20.4%
79.6%
Sound only
Enh.
44.0%
56.0%
Supp.
F
397 sound-resp. units
135 odor-mod. units
Odor mod.
34.0%
66.0%
Sound only
Enh.
48.1%
51.9%
Supp.
B
Enhanced
Suppressed
Sound (control)
Odor+Sound
Avg. Firing Rate Z-scored
Sound Level (dB SNR)
G
Enhanced
Suppressed
C
OMI
Sound Level (dB SNR)
H
D
5 dB SNR
15 dB SNR
Avg. Firing Rate Z-Scored
Time (s)
I
5 dB SNR
25 dB SNR
E
OMI
Acet.
Euc.
J
K
0 dB
Odor
Control
Avg. Firing Rate Z-scored
Control
Odor
L
Sniff Frequency (Hz)
Sniff Amplitude (a.u.)

768

Figure 4. Odor modulates sound responses in auditory cortex. A) Left: Percentage of significantly odor-modulated units in ACx in response to unmodulated broadband noise, according to GLM. Right: percentage of Enhanced vs Suppressed odor-modulated units. n=5 mice (1 C57BL/6J, 4 Cdh23), 368 sound-responsive units, 293 'Sound only' units, 75 'Odor mod.' units, 33 Enhanced units, 42 Suppressed units. **B)** Average responses to sound levels (dB SNR relative to noise of background air flow), with Odor versus control, for Enhanced units (left) and Suppressed units (right). *p<0.05, **p<0.01, ***p<0.001, Wilcoxon signed-rank tests. **C)** Average Odor Modulation Index (OMI) for each sound level, for Enhanced units (left) and Suppressed units (right). *p<0.05, Friedman test. **D)** Average PSTHs in response to 5 dB SNR (left) and 15 dB SNR (right) sound. Dashed magenta line indicates odor valve opening time, gray lines indicate sound stimulus start and stop times. **E)** Average OMI for experiments with acetophenone (Acet.) versus eucalyptus (Euc.), for enhanced units (left; Acet. n=21 units, Euc. n=12 units) and suppressed units (right; Acet. n=17 units, Euc. n=25 units). n.s. Mann-Whitney tests. **F-J)** Same as A-E, for 10 Hz amplitude modulated noise. n= 5 mice, 397 sound-responsive units, 262 'Sound only' units, 135 'Odor mod.' units, 65 Enhanced units, 70 Suppressed units. **G)** *p<0.05, **p<0.01, ***p<0.001, Wilcoxon signed-rank tests. **H)** *p<0.05, Friedman test. **J)** Left: Acet. n=31 units, Euc. n=34 units. Right: Acet. n=33 units, Euc. n=37 units. n.s. Mann-Whitney tests. **K)** Left and middle: Average firing rate (z-scored) for odor-modulated units (10 Hz AM; units in F, n=135 units), in response to Odor versus control, in the absence of sound (0 dB). **p<0.01, Wilcoxon signed-rank test. Right: PSTH from an example odor-modulated unit, in the absence of sound (0 dB). **L)** Left: Average sniff frequency during Odor versus control trials (n=13 recordings). n.s. paired t-test. Right: Average sniff amplitude during Odor versus control trials (n=13 recordings). ***p<0.001, paired t-test.

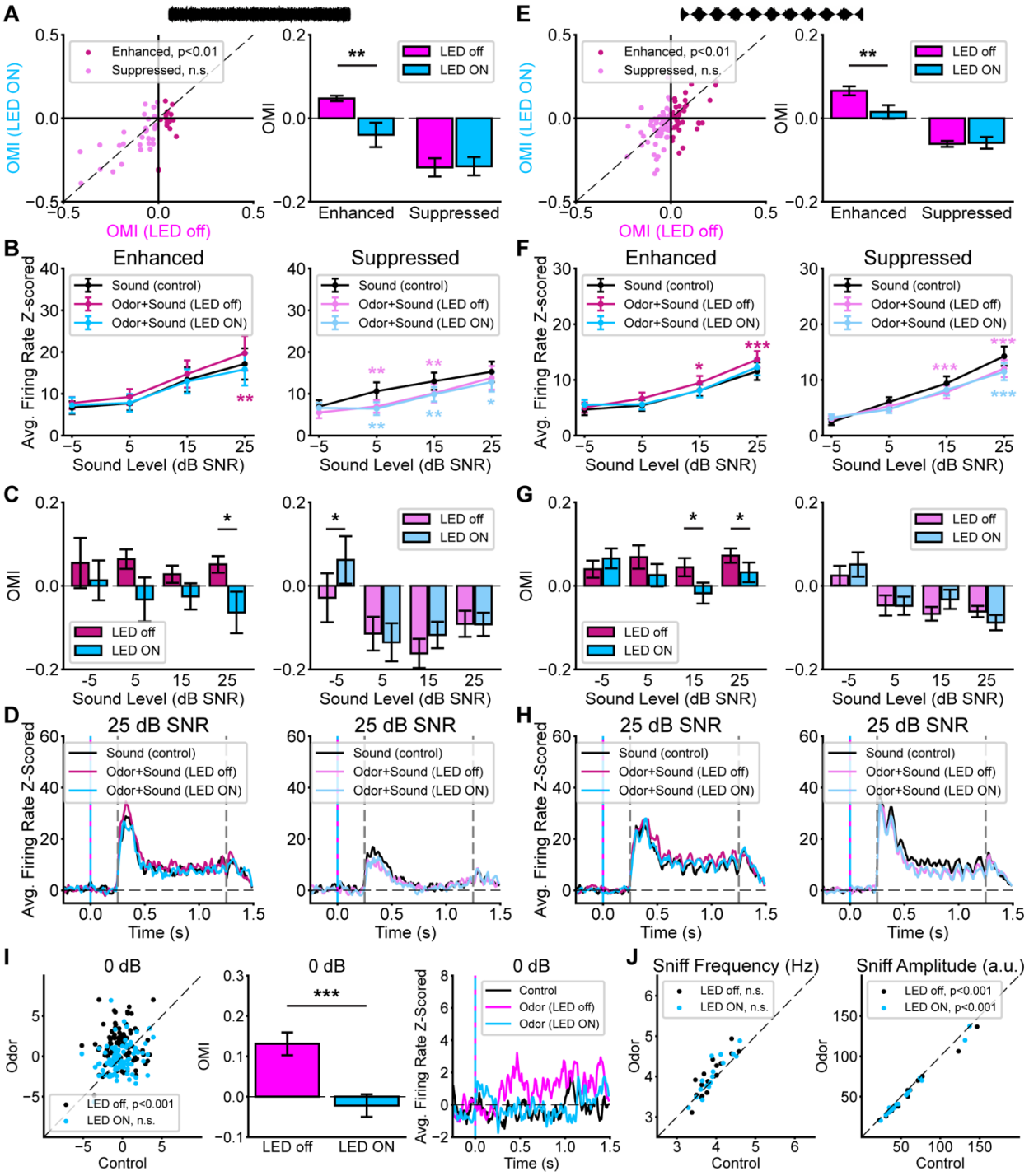

Figure 5. *In vivo* optogenetic inactivation of ACx-projecting piriform neurons reduces odor-mediated enhancement but not suppression. A) Left: Odor Modulation Index (OMI) with vs without LED, for Enhanced and Suppressed ACx units in response to unmodulated broadband noise. n= 6 mice (3 C57BL/6J, 3 Cdh23), 16 Enhanced units, 29 Suppressed units. Wilcoxon

signed-rank tests LED off vs LED ON. Right: Average OMI for Enhanced and Suppressed units, LED off vs LED ON. **p<0.01, Wilcoxon signed-rank test. **B)** Average responses to various sound levels (dB SNR relative to noise of background air flow): sound alone versus odor with or without LED, for Enhanced units (left) and Suppressed units (right). *p<0.05, **p<0.01, Wilcoxon signed-rank tests vs. 'Sound (control)'. **C)** Average OMI for each sound level, for Enhanced units (left) and Suppressed units (right). *p<0.05, Wilcoxon signed-rank test. **D)** Average PSTHs in response to 25 dB SNR sound stimulus. Dashed magenta and cyan lines indicate odor valve opening and LED ON time, gray lines indicate sound stimulus start and stop times. **E-H)** Same as A-D, for 10 Hz amplitude modulated noise. n= 6 mice, 37 Enhanced units, 54 Suppressed units. E) **p<0.01, Wilcoxon signed-rank test. **F)** *p<0.05, ***p<0.001, Wilcoxon signed-rank tests vs. 'Sound (control)' **G)** *p<0.05, Wilcoxon signed-rank tests. **I)** Left: Average firing rate (z-scored) for odor modulated units (10 Hz AM; units in E, n=91 units) in the absence of sound (0 dB), in response to Odor versus control with LED off and LED ON. LED off: ***p<0.001, paired t-test. LED ON: n.s. p>1, Wilcoxon signed-rank test. Middle: Average OMI in the absence of sound (0 dB), LED off vs LED ON, ***p<0.001, Wilcoxon signed-rank test. Right: Average PSTH for odor-modulated units, in the absence of sound (0 dB). **J)** Left: Average sniff frequency during Odor versus control trials, with LED off and LED ON (n=16 recordings). LED off: n.s. LED ON: n.s. paired t-tests. LED off vs LED ON: n.s. paired t-test. Right: Average sniff amplitude during Odor versus control trials (n=13 recordings). LED off: ***p<0.001, LED ON: ***p<0.001, Wilcoxon signed-rank tests. Odor (LED off) vs Odor (LED ON): n.s. Wilcoxon signed-rank test.

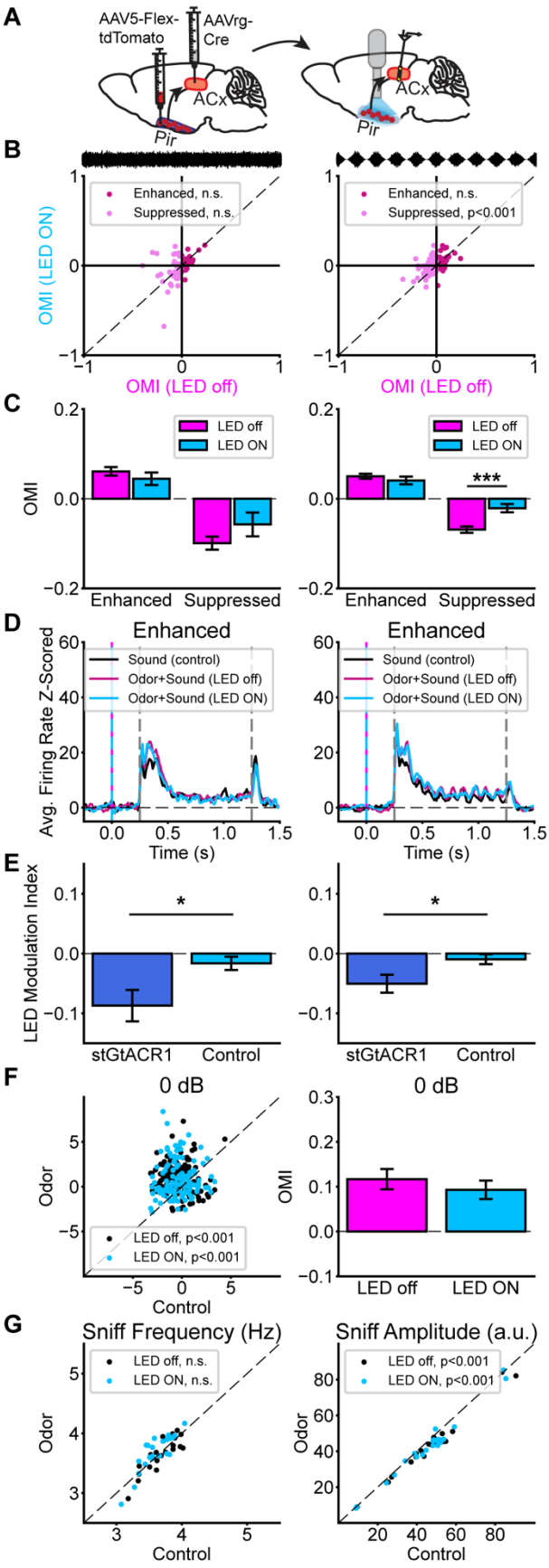
A
AAV5-Flex-tdTomato
AAVrg-Cre
ACx
Pir
B
Enhanced, n.s.
Suppressed, n.s.
Suppressed, p<0.001
OMI (LED ON)
OMI (LED off)
C
LED off
LED ON
OMI
***
Enhanced
Suppressed
D
Enhanced
Sound (control)
Odor+Sound (LED off)
Odor+Sound (LED ON)
Avg. Firing Rate Z-Scored
Time (s)
E
LED Modulation Index
*
stGtACR1
Control
F
0 dB
Odor
Control
LED off, p<0.001
LED ON, p<0.001
OMI
LED off
LED ON
G
Sniff Frequency (Hz)
Sniff Amplitude (a.u.)
LED off, n.s.
LED ON, n.s.
LED off, p<0.001
LED ON, p<0.001
Odor
Control

817

818 **Figure 6. Optogenetic inhibition of odor-mediated enhancement is specifically due to**
819 **inactivation of ACx-projecting Pir neurons. A)** Virus injections for optogenetic control
820 experiments expressing control virus in ACx-projecting Pir neurons in Cdh23 mice. **B)** Left: OMI
821 with vs without LED, for Enhanced and Suppressed ACx units in response to unmodulated
822 broadband noise. n= 7 Cdh23 mice, 29 Enhanced units, 37 Suppressed units. Wilcoxon signed-
823 rank tests LED off vs LED ON. Right: Same as Left, but in response to 10 Hz AM noise. n= 7
824 mice, 60 Enhanced units, 72 Suppressed units. Wilcoxon signed-rank tests LED off vs LED ON.
825 **C)** Average OMI for Enhanced and Suppressed units, LED off vs LED ON., in response to
826 unmodulated noise (left) and 10 Hz AM noise (right). ***p<0.001, Wilcoxon signed-rank test. **D)**
827 Average PSTHs in response to 25 dB SNR sound, for unmodulated (left) and 10 Hz AM noise
828 (right). **E)** LED Modulation Index for Enhanced units in response to unmodulated (left) and 10 Hz
829 AM (right) noise, in stGtACR1 mice versus Control mice. Left: stGtACR1: n=16 units; Control:
830 n=29 units; *p<0.05, Mann-Whitney test. Right: stGtACR1: n=37 units; Control: n=60 units;
831 *p<0.05, Mann-Whitney test. **F)** Left: Average firing rate (z-scored) for odor-modulated units (10
832 Hz AM; units in B, right, n=132 units) in the absence of sound (0 dB), in response to Odor versus
833 control with LED off and LED ON. LED off: ***p<0.001, paired t-test. LED ON: ***p<0.001,
834 Wilcoxon signed-rank test. Right: Average OMI in the absence of sound (0 dB), LED off vs LED
835 ON. n.s. Wilcoxon signed-rank test. **G)** Left: Average sniff frequency during Odor versus control
836 trials, with LED off and LED ON (n=22 recordings). LED off: n.s. paired t-test, LED ON: n.s.
837 Wilcoxon signed-rank test. LED off vs LED ON: n.s. Wilcoxon signed-rank test. Right: Average
838 sniff amplitude during Odor versus control trials (n=22 recordings). LED off: ***p<0.001, LED ON:
839 ***p<0.001, Wilcoxon signed-rank tests. Odor (LED off) vs Odor (LED ON): n.s. Wilcoxon signed-
840 rank test.

841 **Table 1. Statistical comparisons.** Detailed values and statistical tests for all data figures.

Figure	Comparison	Test	n	Test statistic	p-value	Bonferroni corrected p-value
1C	Cell count, aPir vs. pPir	Wilcoxon signed-rank test	7 mice	W = 8	0.38	
1G	Cell count, aPir vs. pPir	Paired t-test	7 mice	t = -3.14	0.020	
2C	Cell count, by Region	Friedman test	6 mice	Q = 10.6	0.014	
4B, left	Enhanced: -5 dB SNR: Sound (control) vs. Odor+Sound	Wilcoxon signed-rank test	33 units	W = 235	0.59	
	Enhanced: 5 dB SNR: Sound (control) vs. Odor+Sound			W = 130.5	0.013	
	Enhanced: 15 dB SNR: Sound (control) vs. Odor+Sound			W = 154	0.023	
	Enhanced: 25 dB SNR: Sound (control) vs. Odor+Sound			W = 127	0.0093	
4B, right	Suppressed: -5 dB SNR: Sound (control) vs. Odor+Sound	Wilcoxon signed-rank test	42 units	W = 357	0.65	
	Suppressed: 5 dB SNR: Sound (control) vs. Odor+Sound			W = 219	0.0061	
	Suppressed: 15 dB SNR: Sound (control) vs. Odor+Sound			W = 128	0.00015	
	Suppressed: 25 dB SNR: Sound (control) vs. Odor+Sound			W = 159	0.00043	
4C, left	Enhanced: OMI, by Sound Level	Friedman test	33 units	Q = 8.36	0.039	
4C, right	Suppressed: OMI, by Sound Level	Friedman test	42 units	Q = 3.46	0.33	
4E, left	Enhanced: OMI, Acet. vs. Euc.	Mann-Whitney test	21 units; 12 units	U = 129	0.93	
4E, right	Suppressed: OMI, Acet. vs. Euc.	Mann-Whitney test	17 units; 25 units	U = 232	0.63	
4G, left	Enhanced: -5 dB SNR: Sound (control) vs. Odor+Sound	Wilcoxon signed-rank test	65 units	W = 983	0.56	
	Enhanced: 5 dB SNR: Sound (control) vs. Odor+Sound			W = 373	8.2e-6	

	Enhanced: 15 dB SNR: Sound (control) vs. Odor+Sound			W = 531	0.0004	
	Enhanced: 25 dB SNR: Sound (control) vs. Odor+Sound			W = 789	0.064	
4G, right	Suppressed: -5 dB SNR: Sound (control) vs. Odor+Sound	Wilcoxon signed-rank test	70 units	W = 819	0.013	
	Suppressed: 5 dB SNR: Sound (control) vs. Odor+Sound			W = 642	0.0012	
	Suppressed: 15 dB SNR: Sound (control) vs. Odor+Sound			W = 661	0.0007	
	Suppressed: 25 dB SNR: Sound (control) vs. Odor+Sound			W = 354	2.0e-7	
4H, left	Enhanced: OMI, by Sound Level	Friedman test	65 units	Q = 9.13	0.028	
4H, right	Suppressed: OMI, by Sound Level	Friedman test	70 units	Q = 3.88	0.27	
4J, left	Enhanced: OMI, Acet. vs. Euc.	Mann-Whitney test	31 units; 34 units	U = 568	0.59	
4J, right	Suppressed: OMI, Acet. vs. Euc.	Mann-Whitney test	33 units; 37 units	U = 624	0.88	
4K	Firing Rate, control vs. Odor	Wilcoxon signed-rank test	135 units	W = 3286	0.0042	
4L, left	Sniff frequency: control vs. Odor	Paired t-test	13 rec.	t = -1.12	0.28	
4L, right	Sniff amplitude: control vs. Odor	Paired t-test	13 rec.	t = 9.43	6.7e-7	
5A	Enhanced: OMI (LED off) vs. OMI (LED ON)	Wilcoxon signed-rank test	16 units	W = 9	0.001	
	Suppressed: OMI (LED off) vs. OMI (LED ON)		29 units	W = 201	0.96	
5B, left	Enhanced: -5 dB SNR: Sound (control) vs. Odor+Sound (LED off)	Paired t-test	16 units	t = -1.14	0.27	0.54
	Enhanced: 5 dB SNR: Sound (control) vs. Odor+Sound (LED off)			t = -1.85	0.085	0.17
	Enhanced: 15 dB SNR: Sound (control) vs. Odor+Sound (LED off)	Wilcoxon signed-rank test		W = 28	0.069	0.14
	Enhanced: 25 dB SNR: Sound (control) vs. Odor+Sound (LED off)			W = 15	0.0042	0.0084

5B, left	Enhanced: -5 dB SNR: Sound (control) vs. Odor+Sound (LED ON)	Wilcoxon signed-rank test	16 units	W = 61	0.74	1.49
	Enhanced: 5 dB SNR: Sound (control) vs. Odor+Sound (LED ON)			W = 62	0.78	1.56
	Enhanced: 15 dB SNR: Sound (control) vs. Odor+Sound (LED ON)			W = 52	0.43	0.87
	Enhanced: 25 dB SNR: Sound (control) vs. Odor+Sound (LED ON)			W = 52	0.43	0.87
5B, right	Suppressed: -5 dB SNR: Sound (control) vs. Odor+Sound (LED off)	Wilcoxon signed-rank test	29 units	W = 155	0.18	0.37
	Suppressed: 5 dB SNR: Sound (control) vs. Odor+Sound (LED off)			W = 53	0.0006	0.0012
	Suppressed: 15 dB SNR: Sound (control) vs. Odor+Sound (LED off)			W = 47	0.0006	0.0012
	Suppressed: 25 dB SNR: Sound (control) vs. Odor+Sound (LED off)			W = 119	0.093	0.19
5B, right	Suppressed: -5 dB SNR: Sound (control) vs. Odor+Sound (LED ON)	Wilcoxon signed-rank test	29 units	W = 206	0.81	1.63
	Suppressed: 5 dB SNR: Sound (control) vs. Odor+Sound (LED ON)			W = 54	0.0007	0.0014
	Suppressed: 15 dB SNR: Sound (control) vs. Odor+Sound (LED ON)			W = 57	0.0009	0.0018
	Suppressed: 25 dB SNR: Sound (control) vs. Odor+Sound (LED ON)			W = 92	0.0056	0.011
5C, left	Enhanced: OMI -5 dB SNR: LED off vs. LED ON	Paired t-test	16 units	t = 1.30	0.21	
	Enhanced: OMI 5 dB SNR: LED off vs. LED ON	Wilcoxon signed-rank test		W = 47	0.30	
	Enhanced: OMI 15 dB SNR: LED off vs. LED ON	Paired t-test		t = 1.31	0.21	
	Enhanced: OMI 25 dB SNR: LED off vs. LED ON			t = 2.22	0.042	
5C, right	Suppressed: OMI -5 dB SNR: LED off vs. LED ON	Wilcoxon signed-rank test	29 units	W = 105	0.044	

	Suppressed: OMI 5 dB SNR: LED off vs. LED ON	Paired t-test		t = 0.49	0.63	
	Suppressed: OMI 15 dB SNR: LED off vs. LED ON	Wilcoxon signed-rank test		W = 171	0.33	
	Suppressed: OMI 25 dB SNR: LED off vs. LED ON			W = 188	0.73	
5E	Enhanced: OMI (LED off) vs. OMI (LED ON)	Wilcoxon signed-rank test	37 units	W = 165	0.0041	
	Suppressed: OMI (LED off) vs. OMI (LED ON)		54 units	W = 636	0.63	
5F, left	Enhanced: -5 dB SNR: Sound (control) vs. Odor+Sound (LED off)	Wilcoxon signed-rank test	37 units	W = 292	0.38	0.76
	Enhanced: 5 dB SNR: Sound (control) vs. Odor+Sound (LED off)			W = 210	0.053	0.11
	Enhanced: 15 dB SNR: Sound (control) vs. Odor+Sound (LED off)			W = 150	0.0069	0.014
	Enhanced: 25 dB SNR: Sound (control) vs. Odor+Sound (LED off)			W = 95	0.0002	0.0004
5F, left	Enhanced: -5 dB SNR: Sound (control) vs. Odor+Sound (LED ON)	Wilcoxon signed-rank test	37 units	W = 222	0.08	0.16
	Enhanced: 5 dB SNR: Sound (control) vs. Odor+Sound (LED ON)			W = 308	0.52	1.04
	Enhanced: 15 dB SNR: Sound (control) vs. Odor+Sound (LED ON)			W = 332	0.78	1.55
	Enhanced: 25 dB SNR: Sound (control) vs. Odor+Sound (LED ON)			W = 294	0.39	0.79
5F, right	Suppressed: -5 dB SNR: Sound (control) vs. Odor+Sound (LED off)	Wilcoxon signed-rank test	54 units	W = 514	0.11	0.22
	Suppressed: 5 dB SNR: Sound (control) vs. Odor+Sound (LED off)			W = 490	0.03	0.06
	Suppressed: 15 dB SNR: Sound (control) vs. Odor+Sound (LED off)			W = 229	1.7e-5	3.3e-5
	Suppressed: 25 dB SNR: Sound (control) vs. Odor+Sound (LED off)			W = 243	1.7e-5	3.4e-5

5F, right	Suppressed: -5 dB SNR: Sound (control) vs. Odor+Sound (LED ON)	Wilcoxon signed-rank test	54 units	W = 490	0.03	0.059
	Suppressed: 5 dB SNR: Sound (control) vs. Odor+Sound (LED ON)			W = 484	0.026	0.052
	Suppressed: 15 dB SNR: Sound (control) vs. Odor+Sound (LED ON)			W = 525.5	0.06	0.12
	Suppressed: 25 dB SNR: Sound (control) vs. Odor+Sound (LED ON)			W = 220	6.8e-6	1.4e-5
5G, left	Enhanced: OMI -5 dB SNR: LED off vs. LED ON	Wilcoxon signed-rank test	37 units	W = 249	0.19	
	Enhanced: OMI 5 dB SNR: LED off vs. LED ON	Paired t-test		t = 1.69	0.11	
	Enhanced: OMI 15 dB SNR: LED off vs. LED ON	Wilcoxon signed-rank test		W = 188	0.013	
	Enhanced: OMI 25 dB SNR: LED off vs. LED ON			W = 199	0.021	
5G, right	Suppressed: OMI -5 dB SNR: LED off vs. LED ON	Wilcoxon signed-rank test	54 units	W = 726	0.89	
	Suppressed: OMI 5 dB SNR: LED off vs. LED ON			W = 710	0.96	
	Suppressed: OMI 15 dB SNR: LED off vs. LED ON			W = 553	0.10	
	Suppressed: OMI 25 dB SNR: LED off vs. LED ON	Paired t-test		t = 1.23	0.26	
5I, left	Firing Rate, control vs. Odor (LED off)	Paired t-test	91 units	t = -5.70	1.5e-7	3.1e-7
	Firing Rate, control vs. Odor (LED ON)	Wilcoxon signed-rank test		W = 1957	0.59	1.18
5I, middle	OMI, LED off vs. LED ON	Wilcoxon signed-rank test	91 units	W = 786	2.3e-7	
5J, left	Freq.: control vs. Odor (LED off)	Paired t-test	16 rec.	t = -2.21	0.043	0.087
	Freq.: control vs. Odor (LED ON)			t = -2.28	0.038	0.076
	Freq.: Odor (LED off) vs. Odor (LED ON)			t = -0.88	0.39	0.78
5J, right	Amp.: control vs. Odor (LED off)	Wilcoxon signed-rank test	16 rec.	W = 0	3.1e-5	6.2e-5
	Amp.: control vs. Odor (LED ON)			W = 4	0.0002	0.0004

	Amp.: Odor (LED off) vs. Odor (LED ON)			W = 41	0.18	0.35
6B-C, left	Enhanced: OMI (LED off) vs. OMI (LED ON)	Wilcoxon signed-rank test	29 units	W = 142	0.11	
	Suppressed: OMI (LED off) vs. OMI (LED ON)		37 units	W = 239	0.14	
6B-C, right	Enhanced: OMI (LED off) vs. OMI (LED ON)	Wilcoxon signed-rank test	60 units	W = 676	0.11	
	Suppressed: OMI (LED off) vs. OMI (LED ON)		72 units	W = 497	7.6e-6	
6E, left	LED Modulation Index, stGtACR1 vs. Control	Mann-Whitney test	16 units; 29 units	U = 125	0.012	
6E, right	LED Modulation Index, stGtACR1 vs. Control	Mann-Whitney test	37 units; 60 units	U = 828	0.037	
6F, left	Firing Rate, control vs. Odor (LED off)	Paired t-test	132 units	t = -6.29	4.3e-9	8.7e-9
	Firing Rate, control vs. Odor (LED ON)	Wilcoxon signed-rank test		W = 2218	8.2e-7	1.6e-6
6F, right	OMI, LED off vs. LED ON	Wilcoxon signed-rank test	132 units	W = 3882	0.31	
6G, left	Freq.: control vs. Odor (LED off)	Paired t-test	22 rec.	t = 0.85	0.40	0.81
	Freq.: control vs. Odor (LED ON)	Wilcoxon signed-rank test		W = 63	0.04	0.08
	Freq.: Odor (LED off) vs. Odor (LED ON)			W = 110	0.61	1.2
6G, right	Amp.: control vs. Odor (LED off)	Wilcoxon signed-rank test	22 rec.	W = 1	9.5e-7	1.9e-6
	Amp.: control vs. Odor (LED ON)			W = 18	0.0001	0.0002
	Amp.: Odor (LED off) vs. Odor (LED ON)			W = 86	0.20	0.40

842